Grant Agreement No.: 604656

Project acronym: NanoSim

Project title: A Multiscale Simulation-Based Design Platform for Cost-Effective CO_2 Capture Processes using Nano-Structured Materials (NanoSim)

Funding scheme: Collaborative Project

Thematic Priority: NMP

THEME: [NMP.2013.1.4-1] Development of an integrated multi-scale modelling environment for nanomaterials and systems by design

Starting date of project: 1st of January, 2014

Duration: 48 months

WP N°	Del. N°	Title	Contributors	Version	Lead beneficiary	Nature	Dissemin. level	Delivery date from Annex I	Actual delivery date dd/mm/yyyy
6	D6.1	Complete generic foundation for steady/transient fluidized bed reactor simulations	Joana Francisco Morgado John Morud Schalk Cloete Thomas Gurker	1	8	D	PU	15	15/04/2016

1 Description

The present document discusses the achievements on the 1D phenomenological model (Phenom) developed for fluidized bed reactors (i.e. code, modelling approach, numerical scheme and test cases).

2 Model overview

Phenom consists of a stand-alone generic 1D phenomenological model for fluidized bed reactors valid under three different fluidization regimes, bubbling, turbulent and fast fluidization (the most used in industry). The model formulation used in Phenom is based on a probabilistic averaging approach [1] that enables a smooth transition between the regimes when combined inside the reactor system (most often the case). This kind of models (phenomenological) have high contribution in industry due to its low CPU requirements, simplicity and reasonable accuracy of the reactor performance predictions. MATLAB was used to develop this code.

2.1 Modelling Approach

The program structure is represented in Figure 1.

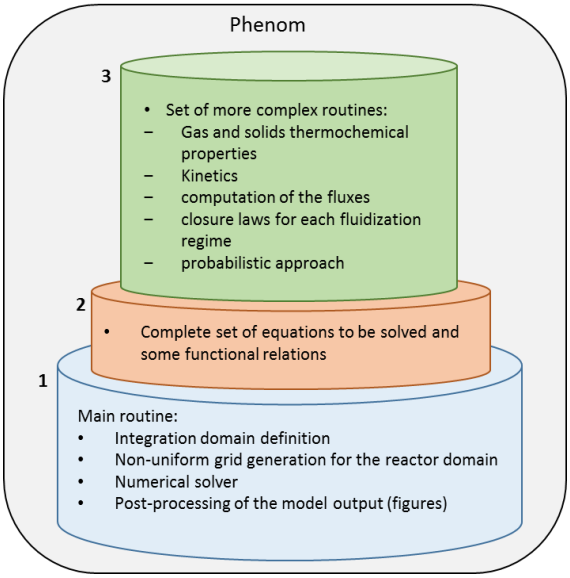

Figure 1 – Code structure: 1) Main program, 2) Reactor model and 3) Model Parameters (based on [2])

As observed in Figure 1 (2-3) modelling of fluidized bed reactors involves an accurate coupling of several phenomena. Firstly, we have the model structure composed by a set of consistent differential balances (mass, energy and pressure) from which the state variables profiles are obtained (*e.g.* gas and solids composition, temperature, pressure). Then, in order to represent the system at the operating conditions under study these balances are coupled with relations with different

degrees of complexity that give information regarding the thermo-chemical properties, geometry, physics and hydrodynamics of the system (the model parameters).

The present model relies on the following assumptions:

1. Formulation can be applied in transient and stationary regime (test cases presented beloow are under stationary conditions);
2. 1D model: only the axial direction is taken into account;
3. Adiabatic system;
4. In the following test cases pressure is assumed to be constant along the reactor;
5. The gas phase comprises two zones, a Low-dense phase with a very low concentrations on solids and High-dense phase with a higher fraction of solids;
6. Axially dispersed flow in both L- and H- phases
7. Heterogeneous model (a total solids balance is incorporated) – a third phase is added to the system.
8. Ideal gas is assumed;
9. Reactor with constant cross-section area;
10. Temperature is uniform in the reactor system (a unique total energy balance is considered);
11. The gas superficial velocity is higher than the minimum fluidization velocity;

The system of equations is described in more detail below.

2.1.1 State variables

w_i^{φ}	Mass fraction of specie *i* in the gas phase φ
	where *i* = CH_4, CO, CO_2, H_2, H_2O, N_2 and $\varphi = H, L$ phases in the gas
$w_{s,k}$	Mass fraction of specie *k* in the solids phase
	where *s* = solid phase and *k* = Ni, NiO, $NiAl_2O_4$, Al_2O_3
T	Temperature of the system (including both gas and solids phase)
U	Superficial velocity of the gas
P	Pressure

Initial conditions, t = 0:

Mass fractions in the gas phase

$w_i(0,z) = w_{i,inlet}$

Mass fractions in the solids phase

$w_{s,k}(0,z) = w_{s,i,inlet}$

$T(0,z) = T_{inlet}$

$U(0,z) = U_{inlet}$

$P(0,z) = P_{inlet}$

2.1.2 Gas phase Equations

- **Ideal gas equation of state**

$$\rho_g = \frac{P}{RT} \quad (1)$$

Pressure balance based on the hydrostatic pressure of the solids.

$$-\frac{\partial P}{\partial z} = (1-\varepsilon)\rho_{w,s}g + \varepsilon\rho_{w,g}g \quad (2)$$

Boundary condition

$(P)_{z=Z} = P_{out}$ (Dirichlet Boundary condition)

- **Material balance for specie i in the H-dense phase** (non-conservative form).

$$\psi_H\varepsilon_H\rho_{w,g}\frac{\partial(w_i^H)}{\partial t} + \psi_H\rho_{w,g}u_H\frac{\partial}{\partial z}(w_i^H) = \frac{\partial}{\partial z}\left(\psi_H\rho_{w,g}D_g\frac{dw_i^H}{dz}\right) + \psi_L K_{LH}\rho_{w,g}(w_i^L - w_i^H) + \Gamma_g^{L\to H}w_i^{up} + \sum_j v_{j,i}r_j^H Mw_i - w_i^H\sum_i R_i^H \quad (3)$$

Where r_j^H corresponds to the rate of the reaction *j* in the gas H-phase and R_i^H to the reaction rate for component *i* in the H-phase.

- **Material balance for specie *i* in the L-dense phase** (non-conservative form).

$$\psi_L\varepsilon_L\rho_{w,g}\frac{\partial(w_i^L)}{\partial t} + \psi_L\rho_{w,g}u_L\frac{\partial(w_i^L)}{\partial z} = \frac{\partial}{z}\left(\psi_L\rho_{w,g}D_g\frac{dw_i^L}{dz}\right) + \psi_L K_{LH}\rho_{w,g}(w_i^H - w_i^L) - \Gamma_g^{L\to H}w_i^{up} + \sum_j v_{j,i}r_j^L Mw_i - w_i^L\sum_i R_i^L \quad (4)$$

Boundary conditions for both phases

***z* = 0** Initial Flux (Equivalent to Danckwerts boundary conditions)

***z* = Z** Zero outlet gradient

- **Total Material balance in the gas phase** (fluxes written in the conservative form as it is easier to find inconsistencies in the balances)

$$\frac{\partial F_{w,Total}}{\partial t} = F_{w,Total}|_{in} + \sum_i R_i \, \Delta z - F_{w,Total}|_{out} \qquad \textbf{5}$$

Where $F_{w,Total} = \sum_i F_{w,i}^L + \sum_i F_{w,i}^H$.

These fluxes at the cell faces are defined as follows.

$$F_{w,i}^{\varphi} = \left(\psi_{\varphi}\rho_{w,g}u_{\varphi}w_i^{\varphi}\right)_s - \left(\psi_{\varphi}\rho_{w,g}D_g^{\varphi}\right)_s \frac{\partial\left(w_i^{\varphi}\right)}{\partial z}$$

This equation is integrated along with the other partial differential equations in order to have a simultaneous update of the velocity given by an algebraic equation.

- **Total energy balance in the non-conservative form**

$$\left[\rho_{w,s}(1-\varepsilon)Cp_s - \rho_{w,g}\varepsilon Cp_g\right]\frac{\partial T}{\partial t} = -\left[F_{h,g} + F_{h,s} - \lambda_{ax}\frac{\partial T}{\partial z}\right] + \sum_j r_j\left(-\Delta H_{r,j}\right) \qquad \textbf{6}$$

The enthalpy fluxes are described in more detail below.

Enthalpy flux for the gas phase: $F_{h,g} = \frac{\partial h_L}{\partial z} + \frac{\partial h_H}{\partial z} = \sum_i\left(F_{w,i}^L Cp_{i,L}\right)\frac{\partial T}{\partial z} + \sum_i\left(F_{w,i}^H Cp_{hi,}\right)\frac{\partial T}{\partial z}$

Enthalpy flux for the solids $F_{h,s} = \frac{\partial h_s}{\partial z} = \sum_k\left(F_{s,k}Cp_s\right)\frac{\partial T}{\partial z}$

Where *k* is the index to specify the species in the solids phase.

Boundary conditions for both phases

***z* = 0** Initial Flux (Equivalent to Danckwerts boundary conditions)

***z* = Z** Zero outlet gradient

2.1.3 Solid phase equation

Total material balance for specie *i* in the solid phase.

$$(1-\varepsilon)\rho_{w,s}\frac{\partial\left(w_{s,k}\right)}{\partial t} + \rho_{w,s}U_s\frac{\partial\left(w_{s,k}\right)}{\partial z} = \frac{\partial}{\partial z}\left(\rho_{w,s}D_s\frac{\partial w_{s,k}}{\partial z}\right) + \sum_j v_{j,k}r_j^s Mw_k - w_{s,i}\sum_k R_k^s \qquad \textbf{7}$$

Where r_j^s corresponds to the rate of the reaction *j* in the solids phase and R_k^s to the reaction rate for component *k* in the solids phase.

Boundary conditions for both phases

***z* = 0** Initial Flux (Equivalent to Danckwerts boundary conditions)

***z* = Z** Zero outlet gradient

The numerical solution of this set of equations results in the state variable profiles: gas and solids composition profiles, temperature profile and the pressure drop along the bed. The model parameters used to describe the hydrodynamics of the system are determined based on closures which are subject to the probabilistic averaging approach proposed in [1].

3 Numerical implementation and solver details

This set of equations results in a Differential Algebraic differential (DAE) problem where all the equations are solved simultaneously. The Finite Volume method was used for spatial discretization (the reactor is divided in small cell volumes).

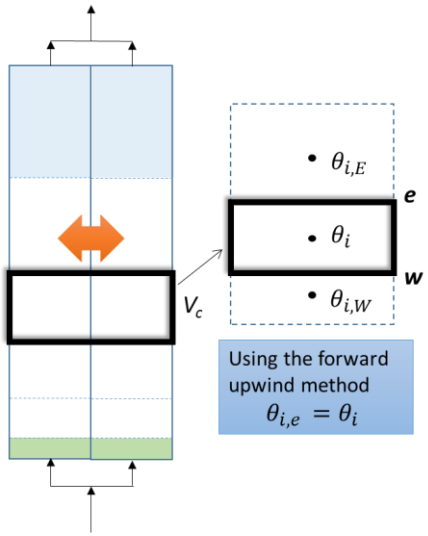

Figure 2- Sketch of a cell volume

A non-uniform grid was considered due to the reaction characteristics. A simple first order upwind scheme was used to compute the convective term of the balances describing the fluxes at the volume cells. The diffusion term is discretized using the central differenced.

The discretized form of the pressure balance (algebraic equation) is the following.

$$0 = (P_e - P) + \left[(1-\varepsilon)\rho_{w,s}g + \varepsilon\rho_{w,g}g\right]\Delta z \qquad 8$$

The discretized form of the non-conservative equations for the species balances in the gas phase (Equation 3 and 4) are from the conservative form as follows.

$$\frac{\partial}{\partial t}\left(\psi_\varphi \varepsilon_\varphi \rho_{w,g} w_i^\varphi\right) + \frac{\partial}{\partial z}\left(\psi_\varphi u_\varphi \rho_{w,g} w_i^\varphi\right) = \frac{\partial}{\partial z}\left(\rho_{w,g} D_g \frac{\partial\left(w_i^\varphi\right)}{\partial z}\right) + S_\varphi \qquad \mathbf{9}$$

By integration over the control volume,

$$\int_{V_c} \frac{\partial}{\partial t}\left(\psi_\varphi \varepsilon_\varphi \rho_{w,g} w_i^\varphi\right) dv + \int_{V_c} \frac{\partial}{\partial z}\left(\psi_\varphi u_\varphi \rho_{w,g} w_i^\varphi\right) dv = \int_{V_c} \frac{\partial}{\partial z}\left(\rho_{w,g} D_g \frac{\partial\left(w_i^\varphi\right)}{\partial z}\right) dv + \int_{V_c} S_\varphi \, dv \quad \textbf{10}$$

$$\Delta z \frac{\partial}{\partial t}\left(\psi_\varphi \varepsilon_\varphi \rho_{w,g} w_i^\varphi\right) + \psi_\varphi u_\varphi \rho_{w,g} w_i^\varphi \Big]_w^e = \rho_{w,g} D_g \frac{\partial\left(w_i^\varphi\right)}{\partial z}\Big]_w^e + S_\varphi \Delta z \quad \textbf{11}$$

$$\begin{aligned} \Delta z \frac{\partial}{\partial t}\left(\psi_\varphi \varepsilon_\varphi \rho_{w,g} w_i^\varphi\right) + \left(\psi_\varphi u_\varphi \rho_{w,g} w_i^\varphi\right)_e - \left(\psi_\varphi u_\varphi \rho_{w,g} w_i^\varphi\right)_w \\ = \left(\rho_{w,g} D_g \frac{\partial\left(w_i^\varphi\right)}{\partial z}\right)_e - \left(\rho_{w,g} D_g \frac{\partial\left(w_i^\varphi\right)}{\partial z}\right)_w + S_\varphi \Delta z \end{aligned} \quad \textbf{12}$$

The sum of the transport equations for all the species involved leads to the continuity equation where the sum of the diffusive mass fluxes vanishes. Therefore, the total mass balance is given as follows:

$$\Delta z \frac{d}{dt}\left(\psi_\varphi \varepsilon_\varphi \rho_{w,g}\right) + \psi_\varphi u_\varphi \rho_{w,g} \Big]_w^e = S_\varphi \Delta z \quad \textbf{13}$$

By multiplying Equation **13** by w_i^φ.

$$\Delta z \frac{d}{dt}\left(\psi_\varphi \varepsilon_\varphi \rho_{w,g}\right) w_i^\varphi + \left(\psi_\varphi u_\varphi \rho_{w,g}\right)_e w_i^\varphi - \left(\psi_\varphi u_\varphi \rho_{w,g}\right)_w w_i^\varphi = S_\varphi \Delta z w_i^\varphi \quad \textbf{14}$$

Using the product rule and subtracting the Equation **12** by **14** the following expression is obtained.

$$\begin{aligned} \Delta z \frac{\partial}{\partial t}\left(\psi_\varphi \varepsilon_\varphi \rho_{w,g}\right) w_i^\varphi + \Delta z \psi_\varphi \varepsilon_\varphi \rho_{w,g} \frac{\partial\left(w_i^\varphi\right)}{\partial t} - \Delta z \frac{d}{dt}\left(\psi_\varphi \varepsilon_\varphi \rho_{w,g}\right) w_i^\varphi + \left(\psi_\varphi u_\varphi \rho_{w,g}\right)_e \left(w_{i,e}^\varphi - w_i^\varphi\right) \\ + \left(\psi_\varphi u_\varphi \rho_{w,g}\right)_w \left(w_{i,w}^\varphi - w_i^\varphi\right) = \left(\rho_{w,g} D_g \frac{\partial\left(w_i^\varphi\right)}{\partial z}\right)_e - \left(\rho_{w,g} D_g \frac{\partial\left(w_i^\varphi\right)}{\partial z}\right)_w + S_\varphi \Delta z - w_i^\varphi S_\varphi \Delta z \end{aligned} \quad \textbf{15}$$

The following equation for specie *i* in the φ-phase is obtained.

$$\begin{aligned} \Delta z \psi_\varphi \varepsilon_\varphi \rho_{w,g} \frac{\partial\left(w_i^\varphi\right)}{\partial t} + \left(\psi_\varphi u_\varphi \rho_{w,g}\right)_e \left(w_{i,e}^\varphi - w_i^\varphi\right) + \left(\psi_\varphi u_\varphi \rho_{w,g}\right)_w \left(w_{i,w}^\varphi - w_i^\varphi\right) \\ = \left(\rho_{w,g} D_g \frac{\partial\left(w_i^\varphi\right)}{\partial z}\right)_e - \left(\rho_{w,g} D_g \frac{\partial\left(w_i^\varphi\right)}{\partial z}\right)_w + S_\varphi \Delta z - w_i^\varphi S_\varphi \Delta z \end{aligned} \quad \textbf{16}$$

Using a simple first order forward upwind scheme $w_{i,e}^\varphi = w_i^\varphi$. Therefore, the following final discretized equation for specie *i* in the φ-phase is obtained.

$$\Delta z \psi_\varphi \varepsilon_\varphi \rho_{w,g} \frac{\partial\left(w_i^\varphi\right)}{\partial t} + \left(\psi_\varphi u_\varphi \rho_{w,g}\right)_w \left(w_{i,w}^\varphi - w_i^\varphi\right) = \left(\rho_{w,g} D_g \frac{\partial\left(w_i^\varphi\right)}{\partial z}\right)_e - \left(\rho_{w,g} D_g \frac{\partial\left(w_i^\varphi\right)}{\partial z}\right)_w + S_\varphi \Delta z - w_i^\varphi S_\varphi \Delta z \quad \textbf{17}$$

The same procedure is used for the species balance discretization in the solids phase. The discretized equation is the following.

$$\Delta z(1-\varepsilon)\rho_{w,s}\frac{\partial(w_{s,k})}{\partial t}+(\rho_{w,s}U_s)_w(w_{s,k,w}-w_{s,k}) = \left(\rho_{w,s}D_s\frac{\partial(w_{s,k})}{\partial z}\right)_e-\left(\rho_{w,s}D_s\frac{\partial(w_{s,k})}{\partial z}\right)_w+S_{sol}\Delta z-w_{s,k}S_{sol}\Delta z \quad (18)$$

The Energy balance discretization

$$\left[\rho_{w,s}(1-\varepsilon)Cp_s-\rho_{w,g}\varepsilon Cp_g\right]\frac{\partial T}{\partial t}+\sum_i\left(F^L_{w,i}Cp_{i,L}\right)\frac{\partial T}{\partial z}+\sum_i\left(F^H_{w,i}Cp_{i,H}\right)\frac{\partial T}{\partial z}+\sum_k\left(F_{s,k}Cp_s\right)\frac{\partial T}{\partial z}+\frac{\partial}{\partial z}\left(\lambda_{ax}\frac{\partial T}{\partial z}\right)=S_\varphi \quad (19)$$

The final discretized Equation is the following.

$$\Delta z\left(\rho_{w,s}(1-\varepsilon)Cp_s-\rho_{w,g}\varepsilon Cp_g\right)\frac{\partial T}{\partial t} = -\left[\sum_i\left(F^L_{w,i}|_w\Delta h_{i,L}+F^H_{w,i}|_w\Delta h_{i,H}\right)+\sum_k F_{s,k}|_w Cp_s(T_w-T)\right]+\left(\lambda_{ax}\frac{\partial(T)}{\partial z}\right)_e-\left(\lambda_{ax}\frac{\partial(T)}{\partial z}\right)_w+S_\varphi \quad (20)$$

Where $\Delta h_{i,L}=h_{i,w}(T)-h_{i,w}(T_W)=\int_{T_W}^{T}Cp_{i,L}dT$ and $\Delta h_{i,H}=h_{i,w}(T)-h_{i,w}(T_W)=\int_{T_W}^{T}Cp_{i,H}dT$

This discretization in space reduced the partial differential equations into a set of ordinary differential equations (ODEs), equations, coupled with algebraic equations that can be solved using a robust ode-solver from the MATLAB library. Such approach is called Method of Lines (MOL). The MATLAB routine *ode15s* was used for the integration in time which also recommend for stiff problems as it is the case (due to stiff chemical reaction kinetics). This routine is a multistep solver based on the backward differentiation formulas (BFD). The differential balances are solved for each volume cell simultaneously. Furthermore, the probabilistic approach used to determine the averaged model parameters is solved for each time integration.

4 Test cases

The following test cases were carefully prepared to prove that the model foundation/structure is working using the averaging probabilistic approach to describe the system hydrodynamics. A set of correlations already validated in literature were used for this purpose.

4.1 Mass conservation

Different tests were performed to verify the conservation of mass and results are shown below in Figure 3 to Figure 7. The Oxygen carrier reduction reactions and catalytic steam methane reforming reactions were simulated.

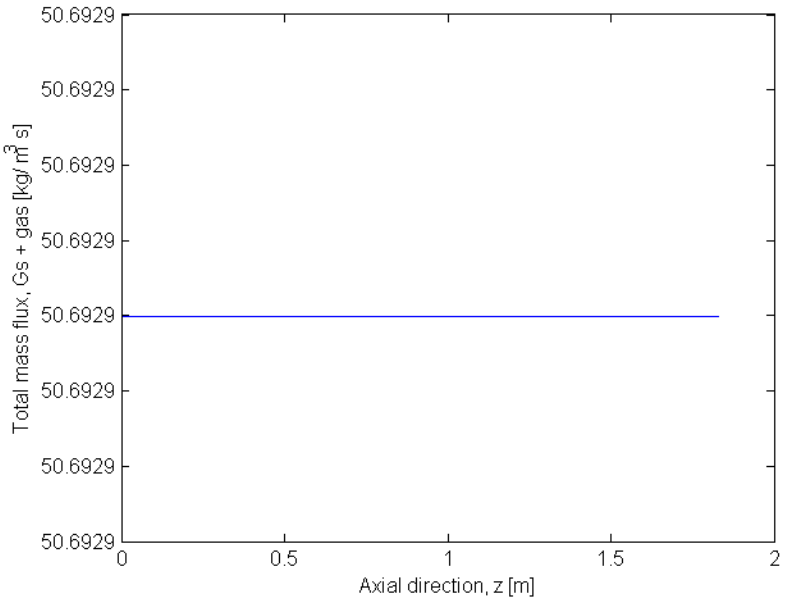

Figure 3 – Total mass Flux along the reactor height

Figure 3 shows that the total mass flux is constant along the height of the reactor assuming that only Ni flux is constant along the bed. It means the matter is conserved over the system.

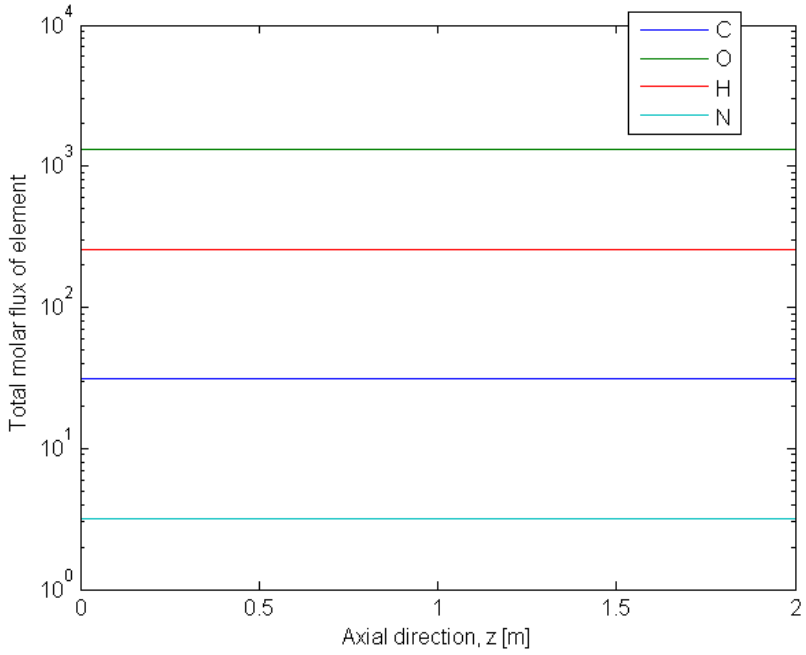

Figure 4 – Total molar fluxes of the element species along the axial direction

Figure 4 shows the total balance of each element present in the reacting species. The total molar flow of each element is constant along the height of the reactor. Therefore, the mass is conserved along the system as concluded before.

Tests were also performed to verify that the flux change in each cell equals to the source terms that include the reaction, bulk transfer and mass transfer. If that is the case, the system behaves as physically expected and conservation of matter is satisfied.

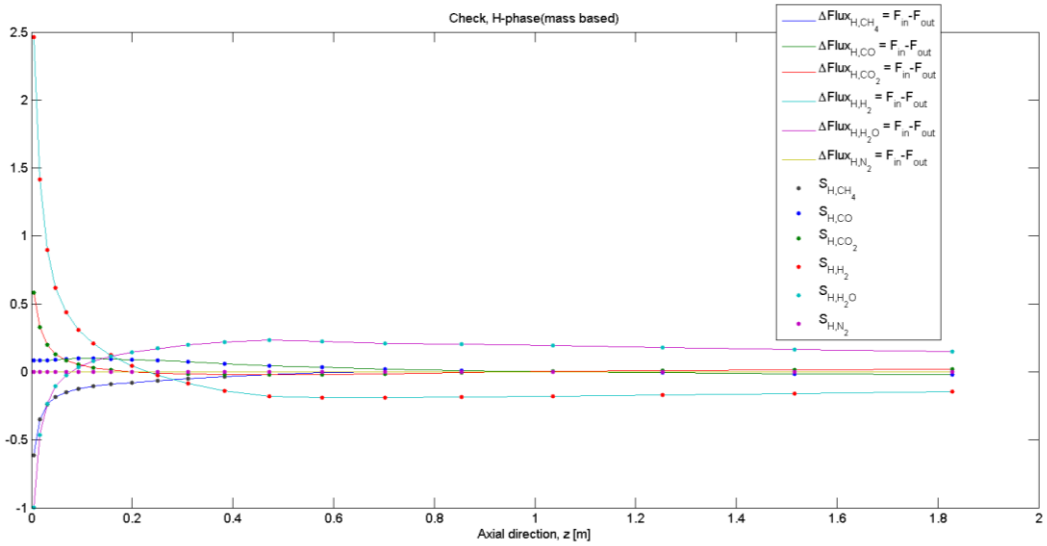

Figure 5 – Agreement between the flux change and source term in each volume cell at the H-phase

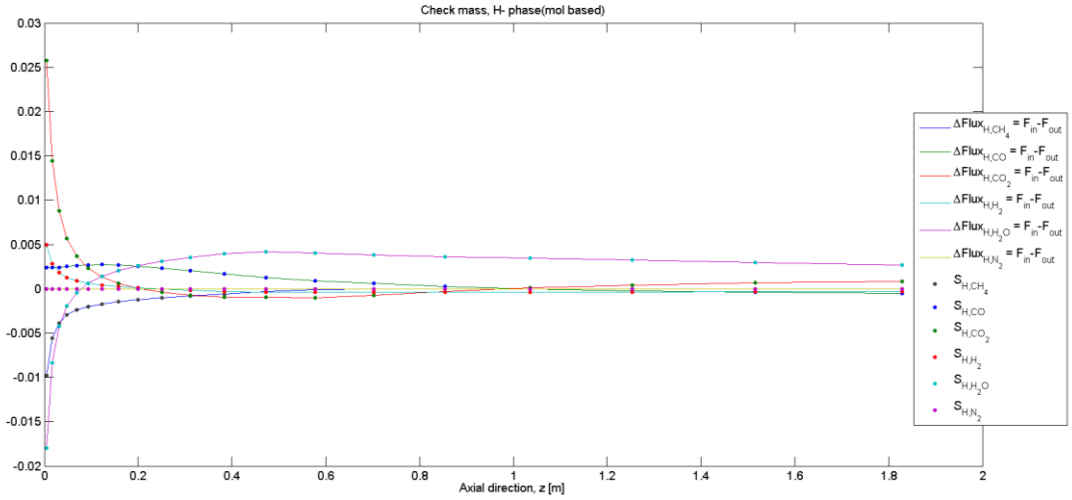

Figure 6 - Agreement between the flux change and source term in each volume cell at the H-phase. In this figure the fluxes and source terms are mole based not mass based as in Figure 5

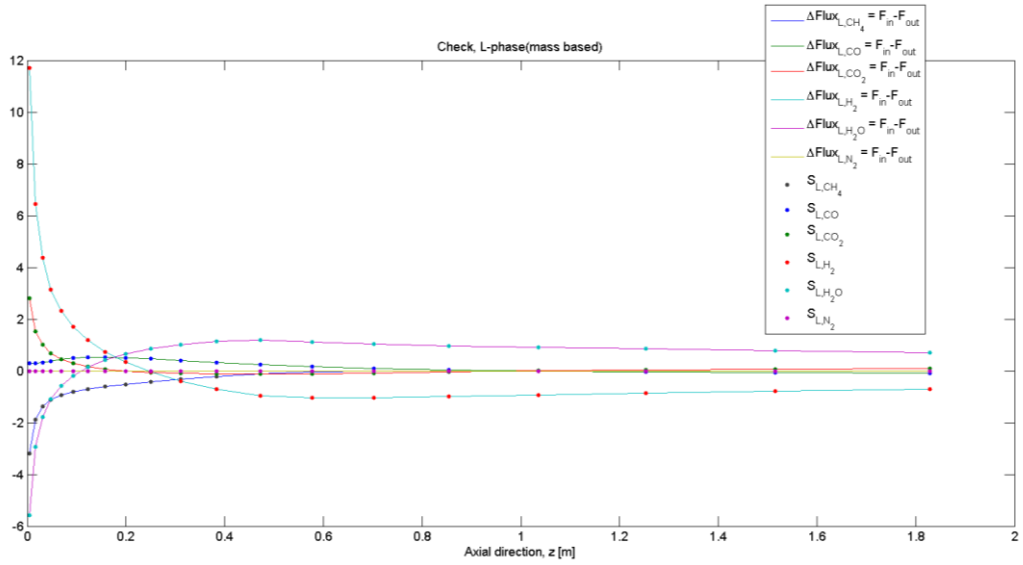

Figure 7 - Agreement between the flux change and source term in each volume cell at the L-phase

As observed in Figure 5, Figure 6 and Figure 7, the source term curves (dots) the flux change (lines) overlap at each cell for both phases, thus confirming that mass is conserved in both phases.

4.2 Energy conservation

If the total change in the enthalpy flux of the reactor streams (gas + solids) equals to the total energy produced/consumed by the reactions at each volume cell, the energy is conserved inside the system (Equation **21**).

$$h_g + h_s = \sum_j \left(-\Delta H_{R,j}\right) R_j \qquad \textbf{21}$$

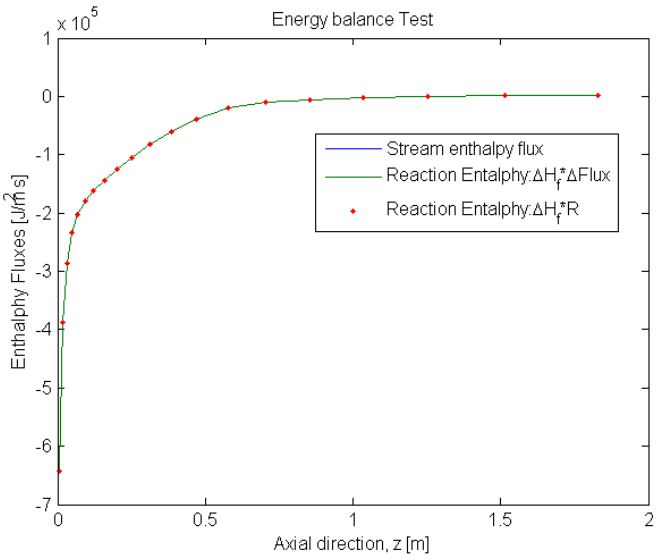

Figure 8 – Energy conservation test

In Figure 8 it is clear that all the curves (red line, blue line and dots) overlap, meaning that the enthalpy change of the stream (gas + particles) in each volume cell equals the total energy that is produced/ consumed in the same volume cell. Therefore, conservation of energy is satisfied.

4.3 CLR reactor simulation example

A Chemical Looping Reforming (CLR) fuel reactor was simulated to illustrate the capabilities of the model. Methane and steam were fed to the reactor along with an oxygen carrier/catalyst (NiO). Catalytic steam methane reforming and water gas shift reactions as well as heterogeneous reduction of the oxygen carrier by fuel gasses were simulated.

Some of the most relevant profiles are presented in Figure 9. Note that the variables were normalized by the maximum value of each variable to allow for visualization of all variables on a single graph.

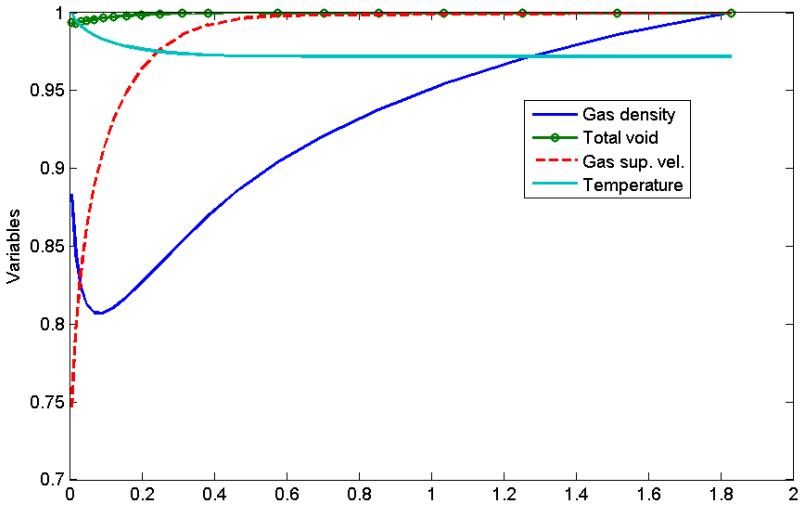

Figure 9 – Relevant Profiles for: Gas density (0.145-0.179 kg/m^3); Total void fraction (0.868-0.874); Gas superficial velocity (4.38-5.88 m/s) and Temperature (752-800 °C)

Figure 9 shows that the profiles for relevant variables in the reactor system qualitatively behave as expected:

Gas density: The gas density decreases during the first 20 cm of the reactor due to the production of H_2 (light gas) from the very fast catalytic steam methane reforming reaction. As the reaction system nears equilibrium and the catalytic reaction slows down, the density increases due to the conversion of H_2 to H_2O in the heterogeneous reduction of NiO to Ni. The decrease in temperature due to endothermic reactions also increases gas density along the height of the reactor.

Total void: The total void slightly increases along the bed due to the increase of the superficial velocity caused by the steam methane reforming reaction. This reaction converts 2 moles of reactants into 4 moles of products. The change in bed voidage is very small due because this effect is cancelled out by the bubble growth rate along the bed. Larger bubbles rise faster, thus requiring a smaller void fraction to maintain the gas flux through the bed.

Gas superficial velocity: The gas superficial velocity increases along the reactor bed due to the increasing of molar flux of the gaseous species created by the steam methane reforming reaction.

Temperature: The temperature of the reactor decreases due to the predominance of endothermic reactions.

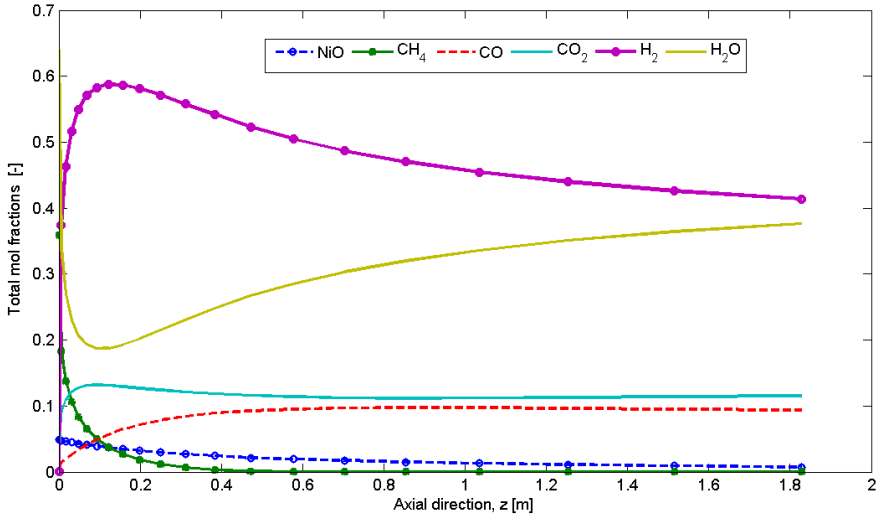

Figure 10 – Composition profiles along the reactor height

Figure 10 shows the composition profiles of the different species present in the reactor. The NiO is slowly reduced (almost at constant rate) until the end of the reactor where it tends to zero. Over the first 20 cm of the reactor length, the reforming reactions are dominant and occur very fast to produce H_2 and consume CH_4. After the initial 20 cm, the catalytic reaction approach equilibrium and the heterogeneous reaction dominates with production of steam and consumption of the H_2 along the reactor bed.

These results show that the model is capable of simulating a CLR reactor system. Any advanced closures (from other work packages in the NanoSim project or the literature) can be easily implemented in the code to further improve predictive capabilities.

5 References

1. Abba, I.a., et al., *Spanning the flow regimes: Generic fluidized-bed reactor model.* AIChE Journal, 2003. **49**: p. 1838-1848.
2. Mahecha-Botero, A., *Comprehensive modelling and its application to simulation of fluidized-bed reactors for efficient production of hydrogen and other hydrocarbon processes*. 2009.